Published in final edited form as:

Pract Radiat Oncol. 2015 ; 5(4): e299–e308. doi:10.1016/j.prro.2014.11.003.

Prospective Observer and Software-based Assessment of Magnetic Resonance Imaging Quality in Head and Neck Cancer: Should Standard Positioning and Immobilization Be Required for Radiotherapy Applications?

Yao Ding, PhD[1,4], **Abdallah S. R. Mohamed, MD, M.sc.**[1,6], **Jinzhong Yang, PhD**[2], **Rivka Colen, MD**[3], **Steven J. Frank, MD**[1,7], **Jihong Wang, PhD**[1,7], **Eslam Y. Wassal, MD, M.Sc.**[3,8], **Wenjie Wang**[2], **Michael E. Kantor, BS**[1], **Peter A. Balter, BS, MS, PhD**[2,7], **David I. Rosenthal, MD**[1], **Stephen Y. Lai, MD, PhD**[5], **John D. Hazle, BS, MS, PhD**[4,7], and **Clifton D. Fuller, MD, PhD**[1,7,*]

[1]Department of Radiation Oncology, The University of Texas MD Anderson Cancer Center, Houston, Texas, USA

[2]Department of Radiation physics, The University of Texas MD Anderson Cancer Center, Houston, Texas, USA

[3]Department of Radiology, The University of Texas MD Anderson Cancer Center, Houston, Texas, USA

[4]Department of Imaging Physics, The University of Texas MD Anderson Cancer Center, Houston, Texas, USA

[5]Department of Head and and Neck Surgery, The University of Texas MD Anderson Cancer Center, Houston, Texas, USA

[6]Department of Clinical Oncology, University of Alexandria, Alexandria, Egypt

[7]The University of Texas Graduate School of Biomedical Sciences, Houston, TX, USA

[8]Department of Diagnostic and Interventional Radiology, Kasr Al-Ainy Faculty of Medicine, Cairo University, Egypt

[*]For correspondence and reprint requests contact: Clifton David Fuller, MD, PhD, The University of Texas MD Anderson Cancer Center, 1515 Holcombe Blvd., Unit 97, Houston, TX, 77030, cdfuller@mdanderson.org.

Conflict of Interest Notification: This work was supported in part by National Institutes of Health Cancer Center Support (Core) Grant CA016672 to The University of Texas MD Anderson Cancer Center. Dr. Ding is funded by a MD Anderson Institutional Research Grant Program. Dr. Mohamed receives salary support from the Union for International Cancer Control /American Cancer Society International Fellowships for Beginning Investigators (UICC/ACSBI) mechanism. Dr. Fuller received/receives grant support from: the National Institutes of Health/National Cancer Institute's Paul Calabresi Clinical Oncology Award Program (K12 CA088084-06) and Clinician Scientist Loan Repayment Program (L30 CA136381-02); the SWOG/Hope Foundation Dr. Charles A. Coltman, Jr., Fellowship in Clinical Trials; a General Electric Healthcare/MD Anderson Center for Advanced Biomedical Imaging In-Kind Award: an Elekta AB/MD Anderson Department of Radiation Oncology Seed Grant; the Center for Radiation Oncology Research at MD Anderson Cancer Center. These listed funders/supporters played no role in the study design, collection, analysis, interpretation of data, manuscript writing, or decision to submit the report for publication.

Abstract

Purpose—To investigate the potential of the head and neck MR-simulation and immobilization protocol on reducing motion induced artifacts and improving positional variance for radiotherapy (RT) applications.

Materials and Methods—Two groups (group one: 17 patients; group two: 14 patients) of head and neck cancer patients were included under a prospective IRB-approved protocol and signed informed consent. 3.0T MRI scanner was used for anatomic and dynamic contrast-enhanced acquisitions using standard diagnostic MRI setup for group 1 and RT immobilization devices for group 2 patients. The impact of MR-simulation/immobilization was evaluated qualitatively by two observers in terms of motion artifacts and positional reproducibility, and quantitatively using three-dimensional deformable registration to track intra-scan maximal motion displacement of voxels inside seven manually segmented regions of interest (ROIs).

Results—The image quality of group 2 (29 exams) was significantly better than that of group 1 (50 exams) as rated by both observers in terms of motion minimization and imaging reproducibility ($P<0.0001$). The greatest average maximal displacement was at the region of the larynx in the posterior direction for patients in group 1 (17mm; SD: 8.6) while the smallest average maximal displacement was at the region of posterior fossa in the superior direction for patients in group 2 (0.4mm; SD: 0.18). Compared to group 1, maximal regional motion at the following ROIs; oral cavity; floor of mouth; oropharynx; and larynx were reduced in group 2 patients, but only in regions of oral cavity and floor of mouth the motion reduction reached statistical significance ($P < 0.0001$).

Conclusions—The image quality of head and neck MRI in terms of motion-related artifacts and positional reproducibility was greatly improved by using the radiotherapy immobilization devices. Consequently, immobilization with external and intra-oral fixation in MRI exams is required for radiotherapy application.

Introduction

Despite recent advances in radiation therapy (RT) including intensity modulated radiotherapy (IMRT) and image guided radiotherapy (IGRT), local and/or regional tumor recurrence still represents a major mode of therapy failure for a considerable portion of head and neck cancer patients (HNC)[1–4]. Identifying areas at higher risk of recurrence within the gross target volume (GTV) with subsequent dose boosting represents a novel strategy that is being investigated recently to reduce the rate of recurrence[5–12].

In an attempt to accurately define and segment those higher risk subvolumes within the gross tumor volume for dose boosting, high quality imaging is crucial. Computed tomography (CT), despite its limitations (e.g. inferior soft tissue contrast and the lack of functional surrogate biomarkers), remains the key component of RT planning process (i.e. tumor and normal tissue delineation, beam/intensity optimization, and dose calculation) due to its superior geometric accuracy and reproducibility in addition to the subsequent dose calculation performed using voxel-based electron density maps. Therefore, all other imaging modalities including magnetic resonance imaging (MRI) and positron emission tomography

(PET) are typically co-registered back to CT for RT planning purposes with varying degrees of error associated with the co-registration process[13–18].

MRI, however, provides much superior soft tissue contrast compared to the standard CT images. Additionally, specific functional MRI biomarkers have been recently introduced as a tool to identify predictive correlates of tumor subvolumes at increased risk for locoregional failures following definitive chemoradiotherapy. Anatomical as well as functional imaging capabilities enabled by MRI represent potential opportunities for improved target delineation, higher risk subvolumes identification and adaptive monitoring of therapy response if properly integrated in RT planning platforms[7,19–21].

Nevertheless, several challenges remain when MRI is incorporated in RT applications either as a primary or secondary imaging modality for HNC. Using MRI as the primary treatment planning tool has the advantage of not having image co-registration induced spatial localization errors yet several other limitations still exist. This include system-related geometric distortions, artifacts caused by motion in the head and neck area, object-induced distortions, and lack of comprehensive electron density information required for dose calculation[22]; therefore, further efforts are required to investigate solutions to overcome these limitations[23–25].

Motion artifacts in HNC MRI studies represent one of these major limitations mentioned above; in addition to bulk head and neck motion, other unavoidable patient movements such as tongue movement, swallowing motion, and breathing may be more problematic during MRI owing to comparatively longer scan time than CT. For standard diagnostic MRI scans, dedicated head and neck coils are used, but immobilization device are typically not used in today's clinical practice.

In order to ensure high quality MRI scan for implementation as a primary RT planning tool as well as for adaptive monitoring of tumor response, our group has developed an immobilization scheme using standard RT positioning and immobilization devices integrated with standard flexible MRI coils, in combination with a flat insert table with indexed base plate, in order to approximate standard RT simulation image requirements. Furthermore, we have implemented a custom dental immobilization apparatus, using a tongue-depressing, mouth opening stent. The stent not only provides a radiotherapy advantage in terms of displacing normal tissues, but also mechanically immobilizes the oral tongue, and prevents gross swallowing motion.

To investigate the potential of this positioning and immobilization technique on reducing motion induced artifacts and improving positional variance for RT applications, we prospectively compared the quality of images acquired using said developed MR-simulation/immobilization protocol to images acquired using our institutional standard diagnostic head and neck MRI (i.e. in the head and neck coil without additional external or intra-oral immobilization).

The specific aims/objectives of the current study include:

1. Qualitative assessment of the impact of MR-simulation/immobilization upon observer assessment of motion artifact and positional reproducibility, using standard MR acquisition without immobilization as a comparator.
2. Quantitative investigation of intra-scan motion using maximal in-scan displacement with deformable image registration software, compared to un-immobilized standard diagnostic scans.
3. Development of a quality assurance (QA) infrastructure for future large-scale standard and functional MRI integration in dose painting RT studies.

Materials and Methods

Study design, setting, and participants

Two groups of head and neck cancer patients with pathologically proven squamous cell carcinoma of the oropharynx were included in this study under a prospective Institutional Review Board (IRB)-approved protocol with signed study-specific informed consent forms. Seventeen patients (Group 1) were scanned between August 2007 and November 2009, as part of a prospective study[26,27], and included anatomic and dynamic contrast-enhanced (DCE) acquisitions. These scans were acquired with a conventional clinical diagnostic head and neck MR imaging protocol and served as the control group for image quality assessment. Fourteen patients (Group 2) were scanned between October 2013 and April 2014 with standardized RT positioning and immobilization head and neck MRI protocol ("MR-simulation") and likewise included both anatomical and DCE-MRI scans, on a separate prospective protocol[28]. All patients were scanned at The University of Texas, MD Anderson Cancer Center. For both protocols, eligible patients were those older than 18 years of age with stage III, IVa, or IVb disease as defined by American Joint Committee on Cancer (AJCC) cancer staging criteria who were dispositioned to receive definitive chemoradiotherapy and with Eastern Cooperative Oncology Group (ECOG) performance status of 0 to 2. Patients were excluded for any of the following reasons: definitive resection of primary tumor or receiving induction chemotherapy before RT; prior cancer diagnosis, except appropriately treated localized epithelial skin cancer or cervical cancer; prior RT to the head-and-neck; patients with any contraindications to gadolinium-based contrast agents; patients with claustrophobia. Patients in both groups were scanned three times: initial scan at baseline prior to the start of RT; a second scan at mid-treatment; and a final scan 8 weeks after the completion of RT. The research for patients in group 2 is on-going with the same time point data acquisition as group 1.

MR Imaging protocol

Imaging in group 1 was performed on a 3.0T GE Signa HDxt MRI scanner (GE Healthcare Wisconsin, WI, USA) using 16-Channel Neurovascular (NV) coil. The patient's head was stabilized in the head cage with foam pads and no additional immobilization was applied, as per standard protocol. The DCE scans (using a cine acquisition) consisted of 3D SPGR (Spoiled Gradient Recalled Echo) sequence to gain sufficient signal-to-noise ratio, contrast and temporal resolution. The following scan parameters were used: flip angle 12°, TE = 1.2 ms, TR = 3.3 ms, NEX = 1, spatial resolution 0.9 mm × 0.9 mm × 3.5 mm, temporal

resolution 5.2 s. After DCE-MRI, T1-weighted contrast enhanced scan (0.1 mmol/kg gadolinium at a rate of 3 mL/s) with fat saturation (TR/TE 700 ms/11 ms; slickness thickness 6.5 mm; FOV 160 mm; matrix 256×160; ETL 1) was obtained in the axial planes.

All data in group 2 were acquired with a 3.0T GE Discovery 750 MRI scanner (GE Healthcare Wisconsin USA) with laterally placed 6-element flex coils centered on the base of tongue region. Patients were fixed to a flat insert table (GE Healthcare Wisconsin USA) during MR scanning with the same RT immobilization devices including individualized thermoplastic head and shoulder mask, customized foam mold head support, and customized intra-oral dental stent. Geometrical scan parameters were accurately prescribed on the same region from the palatine process region cranially to the hypopharynx caudally for each patient. The DCE-MRI scans consisted of 3D SPGR sequence to gain sufficient signal-to-noise ratio, contrast and temporal resolution. The following scan parameters were used: flip angle 15°, TE = 1.0 ms, TR = 3.6 ms, NEX = 0.7, spatial resolution 2 mm × 2 mm × 4 mm, temporal resolution 5.6 s. After cine-MRI (0.1 mmol/kg gadolinium at a rate of 3 mL/s), T1-weighted post contrast scan with fat saturation (TR/TE 600 ms/7 ms; slickness thickness 2.5 mm; FOV 256 mm; matrix 256×256; ETL 2) was obtained in the axial planes. Fig. 1 shows photographs depicting the differences between patient setup before MRI acquisition in both groups.

Image Analysis

Qualitative analysis—Two experts (1 radiologist [XXX] and 1 radiation oncologist [XXX] with 9 and 7 years of experience, respectively, in MR imaging and head and neck radiation treatment) analyzed image quality. Quality scores were given on a three-point scale for head motion artifact (1- major artifact; 2- moderate artifact; 3- minimal or no visible artifact), blur/ghosting around base tongue (1- major blur/ghosting; 2- moderate blur/ghosting; 3- minimal or no visible blur/ghosting), and serial reproducibility of position across pre-, mid, and post-therapy acquisitions (1- poorly reproducible; 2- moderately reproducible; 3- well reproducible). An example of T1-weighted post-contrast images acquired in group1 and group 2 is shown in Fig. 2 for baseline and mid-treatment scans.

Quantitative motion analysis—In attempt to quantitatively assess the impact of the investigated position and immobilization platform on motion magnitude in different regions of the head and neck, seven head and neck reference regions of interest (ROIs) were manually segmented by a radiation oncologist [XXX] on the 1st phase of each pre-contrast cine-MRI for all available DCE scans (Fig. 3). Segmented ROIs were as follows: posterior cranial fossa; oral cavity; floor of mouth; oropharynx; larynx; right and left neck deep cervical neck chain “nodal levels II, III, and IV” (guidelines for manual segmentation boundaries are illustrated in Table 1). These ROIs were automatically registered and tracked in subsequent frames by use of an in-house deformable image registration (DIR) tool using an accelerated Demons algorithm [29,30]. The implemented DIR method has previously been validated for intra-modality head and neck image registration, with more than 99% voxels showing <2mm vector error[31]. In this study, we also directly performed expert-observer assessment of the deformed contours against the underlying anatomical structures in subsequent frames of several patients for post hoc validation[31]. The motion trajectory for

voxels inside each ROI was calculated and used to estimate the motion magnitude. For each patient at each voxel, the motion magnitude was calculated from the motion trajectory as the average displacement to the initial phase of the cine-MRI in each directions – left-right (LR), anterior-posterior (AP), and superior-inferior (SI), and the total motion magnitude was given as

$$M\tau = \sqrt{M_{LR}^2 + M_{AP}^2 + M_{SI}^2}$$

where M_{LR}, M_{AP}, and M_{SI} are the voxel displacement in the LR, AP, and SI directions, respectively). Within each ROI, the mean and standard deviation of the motion magnitude were calculated over all voxels. Finally, the mean, standard deviation, and range of these values were calculated for the each group patient population. We also computed the average maximal ROI motion by taking the average from all vector fields for all voxels to generate average independently for each ROI.

Statistical analysis

All analyses were executed with JMP v 11Pro (SAS institute, Cary, NC). Qualitative assessment of image quality was performed by using Mann-Whitney test between Group1 and Group2 in terms for ordinal scores from both reviewers, matching for subject. Observer agreement was assessed using the kappa agreement statistics; kappa value of 0.21 –0.40 denotes fair agreement; 0.41– 0.60, moderate agreement; 0.61 –0.80, substantial agreement; and 0.81 –1.0, almost perfect agreement.

Intra-scan ROI movement was determined for each patient quantitatively as described above. After confirmation using Shapiro-Wilks assessment to assure normality, a 2-sample t-test was also used to assess differences in motion between both Group1/Group2 in each specific segmented sub-region ROI. For all statistical tests performed, $\alpha < 0.05$ was considered statistically significant.

Results

Patients

A total of thirty patients were eligible; seventeen in group 1 and thirteen in group 2 after exclusion of one patient in group 2 who quit the study during the pre-treatment MRI scan due to poor tolerance to long scan time. Sixteen out of seventeen patients in group 1 underwent the initial, mid-treatment, and follow up exams while one patient was scanned only twice leading to a total of 50 exams; in group 2, six out of thirteen patients completed the three exams; four patients were scanned twice; and three patients were scanned only once leading to a total of 29 MRI exams at the time of the analysis. Patients and disease characteristics are summarized in a Table 2.

Qualitative analysis outcome

The image quality in terms of motion-related artifacts and co-registration was greatly improved by using the RT immobilization devices (Fig. 2). High SNR images were obtained

in group 1 but images acquired with NV coil were not acceptable for RT purposes. Group 2 (29 exams) applied with RT immobilization devices showed significantly better reproducibility over group 1 (50 exams) as rated by both observers ($P<0.0001$ for both.) Likewise, significant motion reduction around both head and tongue regions was also achieved in group 2 as rated by both observers (head motion: P<0.0001 [XXX] and 0.0002 [XXX]; tongue blur: P<0.0001 for both). The overall image quality of group 2 was significantly better than that of group 1 (Table 3) in terms of motion minimization and imaging reproducibility (P<0.0001). Furthermore, no noticeable additional susceptibility artifact is induced by using these immobilization devices. Kappa agreement coefficient between observers for head motion, tongue blur, reproducibility, and overall assessment was 0.34, 0.55, 0.61, and 0.55, respectively.

Quantitative analysis outcome

The greatest total regional motion for each group is summarized in Table 4. The greatest of the average maximum displacement was at the region of the larynx in the posterior direction for patients in group 1 (17mm; SD: 8.6) while the smallest of the average maximum displacement was at the region of posterior fossa in the superior direction for patients in group 2 (0.4mm; SD: 0.18). Overall, compared to group 1, head and neck maximal regional motion at the following ROIs; oral cavity; floor of mouth; oropharynx; and larynx were reduced in group 2 patients, but only motion control in regions of oral cavity and floor of mouth reached statistical significance (P < 0.0001 for both).

Discussion

To the best of our knowledge, this study presents the first investigation of the effect of specific patient positioning and immobilization on the quality of MRI acquired for use in head and neck RT applications. We sought to address the feasibility of obtaining reproducible high-quality MR images using a standardized head and neck RT positioning and immobilization setup. To incorporate MRI as a primary imaging modality for RT application, a better quality image with less motion-induced artifacts is needed. Additionally, to achieve a precise adaptive MRI assessment of tumor response to therapy across time, it is essential to obtain a highly reproducible position to be able to register and track images acquired at different time points. Currently, CT simulation scan with immobilization setup is used for treatment planning and dose calculations, with the same procedure is applied on daily treatment sessions to irradiate the same treatment position. In this study, this identical immobilization setup procedure is applied on MRI practices.

Our results showed that with the use of a set of flexible surface coils, attached to customized mask and mold fixed to a base plate indexed to a flat table top with a customized dental stent, reduced motion and resulted in more reproducible MR images. MR simulation images can be acquired more consistently, compared to images acquired using standard head and neck MRI coils as assessed, qualitatively using observer rating and quantitatively using software deformable image registration evaluation. Generally, both observers denoted better quality of images in Group 2 (immobilized) patients, but showed moderate agreement between both observers across different scans (Kappa =0.55). A quantitative non-observer

dependent method of assessment was, therefore, useful to confirm observer's findings in terms of motion detection. Maximum motion, as expected was primarily due to swallowing, namely in the larynx and oropharynx followed by the oral cavity and floor of mouth. Group 2 fixation methods significantly limited motion at the site of the oral cavity and floor of mouth, and to a lower extent, for oropharynx and larynx ROIs. Furthermore, the addition of intra-oral devices, and equivalent neck positioning substantively increased practical feasibility of MR-CT registration. As illustrated in Fig. 4, the addition of a dental stent and alteration of neck position at simulation necessarily resulted in systematic registration error between CT-simulation and Group 1 MRI scans.

The presented study, however, has typical limitations, including relatively small number of patients, reflecting our initial experience and the need for protocol optimization. Additionally, imaging acquisition protocols were not identical in group 1 and 2 patients which represent a potential confounding factor. As always observer dependencies in image-assessment and ROI delineation must be noted specifically for qualitative assessment as observers could not be blinded due to the apparent differences in scans for both groups because of the presence of the customized dental stent in the scans of patients in group 2 and its absence in group 1. However, the quantitative component of image assessment precludes this potential source of bias. Given our sample distribution, no sub-analyses were performed regarding gender differentials in swallowing magnitude. Nevertheless, as all patients were imaged under prospective protocols with rigorous quality assurance at acquisition, as well as experienced physician observers undertaking analytic efforts, we feel the generalizability of this data remains unhampered by these caveats.

Previous reports comparing MRI displacement reduction and reproducibility improvement, referencing standard diagnostic versus MR simulation positioning and immobilization platforms are sparse. One study recently reported by Verduijn et al showed that the use of the flexible surface coils offer a good alternative to allow the presence of the immobilization mask in head and neck single acquisition MRI exam[32]. While, another study reported by Partridge et al addressed the utility of immobilization for image-registration and multi-modality reproducibility of position over time and concluded that thermoplastic immobilization masks can be used to accurately align multimodality functional image data for assessment of the response to treatment in head and neck patients over extended follow-up periods[33]. However, to our knowledge, this is the first study to demonstrate qualitative and quantitative reduction in patient motion, reduction in motion artifact, and improvement in positional reproducibility across time-points compared to standard diagnostic imaging using both external and intra-oral fixation for MR-simulation.

As MR-radiotherapy technical applications[34,35] as well as functional imaging assessments over the course of therapy[36–40] require spatially accurate images over serial acquisitions, we believe that standardized immobilization for motion artifact control, anatomic motion reduction, and positional reproducibility require MR-simulation for head and neck in a manner analogous to that described. We therefore recommend that specific MR-simulations be acquired for head and neck patients, independent of diagnostic imaging acquisition, when MR is to be used as an input for therapy planning and target delineation.

Conclusions

RT positioning and immobilization platform successfully limited maximal displacements caused by motion in different head and neck regions which was reflected in improved quality, reproducibility and reduced artifacts compared to standard acquisition. Consequently, for those radiotherapy patients for whom integration of MR images with radiation treatment planning is desired, or for whom serial MR scans are indicated, immobilization with external and intra-oral fixation is required for optimized image-quality and reproducibility.

Acknowledgments

Authors are sincerely thankful to Paul Wisdom and the rest of machine shop team at the department of radiation oncology, MD Anderson Cancer Center for the magnificent assistance in constructing the MR immobilization platform. We also wish to thank the Center for Advanced Biomedical Imaging technician team (Jerrell Jones, Logronio Jr Clemente, Brandy Reed, Michelle Underwood, and David Timothy Evans), and Ken-Pin Hwang from imaging physics for their great efforts in acquiring study patient's MR scans. Dr Mohamed acknowledges his support by a UICC American Cancer Society Beginning Investigators Fellowship funded by the American Cancer Society.

References

1. Chao KS, Ozyigit G, Tran BN, Cengiz M, Dempsey JF, Low DA. Patterns of failure in patients receiving definitive and postoperative IMRT for head-and-neck cancer. International journal of radiation oncology, biology, physics. Feb 1; 2003 55(2):312–321.
2. Eisbruch A, Marsh LH, Dawson LA, et al. Recurrences near base of skull after IMRT for head-and-neck cancer: implications for target delineation in high neck and for parotid gland sparing. International journal of radiation oncology, biology, physics. May 1; 2004 59(1):28–42.
3. Schoenfeld GO, Amdur RJ, Morris CG, Li JG, Hinerman RW, Mendenhall WM. Patterns of failure and toxicity after intensity-modulated radiotherapy for head and neck cancer. International journal of radiation oncology, biology, physics. Jun 1; 2008 71(2):377–385.
4. Dawson LA, Anzai Y, Marsh L, et al. Patterns of local-regional recurrence following parotid-sparing conformal and segmental intensity-modulated radiotherapy for head and neck cancer. International journal of radiation oncology, biology, physics. Mar 15; 2000 46(5):1117–1126.
5. Madani I, Duthoy W, Derie C, et al. Positron emission tomography-guided, focal-dose escalation using intensity-modulated radiotherapy for head and neck cancer. Int J Radiat Oncol. May 1; 2007 68(1):126–135.
6. Madani I, Duprez F, Boterberg T, et al. Maximum tolerated dose in a phase I trial on adaptive dose painting by numbers for head and neck cancer. Radiother Oncol. Dec; 2011 101(3):351–355. [PubMed: 21742392]
7. Houweling AC, Wolf AL, Vogel WV, et al. FDG-PET and diffusion-weighted MRI in head-and-neck cancer patients: Implications for dose painting. Radiother Oncol. Feb; 2013 106(2):250–254. [PubMed: 23395065]
8. Chang JH, Wada M, Anderson NJ, et al. Hypoxia-targeted radiotherapy dose painting for head and neck cancer using F-18-FMISO PET: A biological modeling study. Acta Oncol. Nov; 2013 52(8): 1723–1729. [PubMed: 23317145]
9. Berwouts D, Olteanu LAM, Duprez F, et al. Three-phase adaptive dose-painting-by-numbers for head-and-neck cancer: initial results of the phase I clinical trial. Radiother Oncol. Jun; 2013 107(3): 310–316. [PubMed: 23647760]
10. Duprez F, De Neve W, De Gersem W, Coghe M, Madani I. Adaptive Dose Painting by Numbers for Head-and-Neck Cancer. Int J Radiat Oncol. Jul 15; 2011 80(4):1045–1055.
11. Grosu A, Piert M, Souvatzoglou M, et al. Hypoxia Imaging with 18F-FAZA-PET for dose painting using intensity modulated radiotherapy in patients with head and neck cancer. Int J Radiat Oncol. 2005; 63(2):S132–S133.

12. Thorwarth D, Eschmann SM, Paulsen F, Alber M. Hypoxia dose painting based on functional FMISO PET imaging for head-and-neck cancer patients: A feasibility study. Int J Radiat Oncol. 2006; 66(3):S186–S186.
13. Olteanu LA, Madani I, De Neve W, Vercauteren T, De Gersem W. Evaluation of deformable image coregistration in adaptive dose painting by numbers for head-and-neck cancer. International journal of radiation oncology, biology, physics. Jun 1; 2012 83(2):696–703.
14. Manon R, Langen K, Meeks S, et al. Clinical application of deformable image registration in head and neck cancer radiotherapy: Does planned dose to tumor and normal structures change during treatment? Int J Radiat Oncol. 2006; 66(3):S416–S416.
15. Ireland RH, Dyker KE, Barber DC, et al. Nonrigid image registration for head and neck cancer radiotherapy treatment planning with PET/CT. Int J Radiat Oncol. Jul 1; 2007 68(3):952–957.
16. Daisne JF, Sibomana M, Bol A, Cosnard G, Lonneux M, Gregoire V. Evaluation of a multimodality image (CT, MRI and PET) coregistration procedure on phantom and head and neck cancer patients: accuracy, reproducibility and consistency. Radiother Oncol. Dec; 2003 69(3):237–245. [PubMed: 14644482]
17. Nishioka T, Shiga T, Shirato H, et al. Image fusion between (18)FDG-PET and MRI/CT for radiotherapy planning of oropharyngeal and nasopharyngeal carcinomas. Int J Radiat Oncol. Jul 15; 2002 53(4):1051–1057.
18. Rasch C, Keus R, Pameijer FA, et al. The potential impact of CT-MRI matching on tumor volume delineation in advanced head and neck cancer. Int J Radiat Oncol. Nov 1; 1997 39(4):841–848.
19. Kim S, Loevner L, Quon H, et al. Diffusion-weighted magnetic resonance imaging for predicting and detecting early response to chemoradiation therapy of squamous cell carcinomas of the head and neck. Clinical cancer research : an official journal of the American Association for Cancer Research. Feb 1; 2009 15(3):986–994. [PubMed: 19188170]
20. Hatakenaka M, Nakamura K, Yabuuchi H, et al. Pretreatment apparent diffusion coefficient of the primary lesion correlates with local failure in head-and-neck cancer treated with chemoradiotherapy or radiotherapy. International journal of radiation oncology, biology, physics. Oct 1; 2011 81(2):339–345.
21. Lambrecht M, Van Calster B, Vandecaveye V, et al. Integrating pretreatment diffusion weighted MRI into a multivariable prognostic model for head and neck squamous cell carcinoma. Radiother Oncol. Mar; 2014 110(3):429–434. [PubMed: 24630535]
22. Khoo VS, Dearnaley DP, Finnigan DJ, Padhani A, Tanner SF, Leach MO. Magnetic resonance imaging (MRI): Considerations and applications in radiotherapy treatment planning. Radiother Oncol. Jan; 1997 42(1):1–15. [PubMed: 9132820]
23. Walker A, Liney G, Metcalfe P, Holloway L. MRI distortion: considerations for MRI based radiotherapy treatment planning. Australasian physical & engineering sciences in medicine / supported by the Australasian College of Physical Scientists in Medicine and the Australasian Association of Physical Sciences in Medicine. Mar; 2014 37(1):103–113.
24. Prabhakar R, Julka PK, Ganesh T, Munshi A, Joshi RC, Rath GK. Feasibility of using MRI alone for 3D radiation treatment planning in brain tumors. Jpn J Clin Oncol. Jun; 2007 37(6):405–411. [PubMed: 17635965]
25. Crijns SPM, Bakker CJG, Seevinck PR, de Leeuw H, Lagendijk JJW, Raaymakers BW. Towards inherently distortion-free MR images for image-guided radiotherapy on an MRI accelerator. Phys Med Biol. Mar 7; 2012 57(5):1349–1358. [PubMed: 22349351]
26. Bosca RJ, Jackson EF, Dong L, Schwartz DL. Prospective Pharmacokinetic and Diffusion MRI Measurement of Normal Tissue Response to Head and Neck IMRT. Int J Radiat Oncol. 2010; 78(3):S118–S118.
27. Garden, A. A Pilot Trial of Image-Guided Adaptive Radiotherapy for Head and Neck Cancer. ClinicalTrials.gov. Identifier: NCT00490282; https://clinicaltrials.gov/ct2/show/NCT00490282?term=head+neck+garden&rank=3. last access in 6.13.2014
28. Frank, SJ. Intensity-Modulated Proton Beam Therapy (IMPT) Versus Intensity-Modulated Photon Therapy (IMRT). ClinicalTrials.gov. Identifier: NCT01893307; https://clinicaltrials.gov/ct2/show/NCT01893307?term=head+neck+frank&rank=2. M.D. Anderson Cancer Center; last access 6.13.2014

29. Palmer J, Yang J, Pan T, Court LE. Motion of the esophagus due to cardiac motion. PloS one. 2014; 9(2):e89126. [PubMed: 24586540]
30. Wang H, Dong L, Lii MF, et al. Implementation and validation of a three-dimensional deformable registration algorithm for targeted prostate cancer radiotherapy. International journal of radiation oncology, biology, physics. Mar 1; 2005 61(3):725–735.
31. Wang H, Dong L, O'Daniel J, et al. Validation of an accelerated 'demons' algorithm for deformable image registration in radiation therapy. Physics in medicine and biology. Jun 21; 2005 50(12):2887–2905. [PubMed: 15930609]
32. Verduijn GM, Bartels LW, Raaijmakers CP, Terhaard CH, Pameijer FA, van den Berg CA. Magnetic resonance imaging protocol optimization for delineation of gross tumor volume in hypopharyngeal and laryngeal tumors. International journal of radiation oncology, biology, physics. Jun 1; 2009 74(2):630–636.
33. Partridge M, Powell C, Koopman M, Vidan LH, Newbold K. Technical note: 9-month repositioning accuracy for functional response assessment in head and neck chemoradiotherapy. Brit J Radiol. Dec; 2012 85(1020):1576–1580. [PubMed: 23175480]
34. Raaymakers BW, Lagendijk JJ, Overweg J, et al. Integrating a 1.5 T MRI scanner with a 6 MV accelerator: proof of concept. Phys Med Biol. Jun 21; 2009 54(12):N229–237. [PubMed: 19451689]
35. Kron T, Eyles D, John SL, Battista J. Magnetic resonance imaging for adaptive cobalt tomotherapy: A proposal. J Med Phys. Oct; 2006 31(4):242–254. [PubMed: 21206640]
36. Chen Y, Liu X, Zheng D, et al. Diffusion-weighted magnetic resonance imaging for early response assessment of chemoradiotherapy in patients with nasopharyngeal carcinoma. Magn Reson Imaging. Jul; 2014 32(6):630–637. [PubMed: 24703576]
37. Marzi S, Forina C, Marucci L, et al. Early radiation-induced changes evaluated by intravoxel incoherent motion in the major salivary glands. J Magn Reson Imaging. Apr 3.2014
38. Lambrecht M, Van Calster B, Vandecaveye V, et al. Integrating pretreatment diffusion weighted MRI into a multivariable prognostic model for head and neck squamous cell carcinoma. Radiother Oncol. Mar; 2014 110(3):429–434. [PubMed: 24630535]
39. Lambrecht M, Van Herck H, De Keyzer F, et al. Redefining the target early during treatment. Can we visualize regional differences within the target volume using sequential diffusion weighted MRI? Radiotherapy and oncology : journal of the European Society for Therapeutic Radiology and Oncology. Feb; 2014 110(2):329–334. [PubMed: 24231234]
40. Schakel T, Hoogduin JM, Terhaard CH, Philippens ME. Diffusion weighted MRI in head-and-neck cancer: geometrical accuracy. Radiotherapy and oncology : journal of the European Society for Therapeutic Radiology and Oncology. Dec; 2013 109(3):394–397. [PubMed: 24183864]

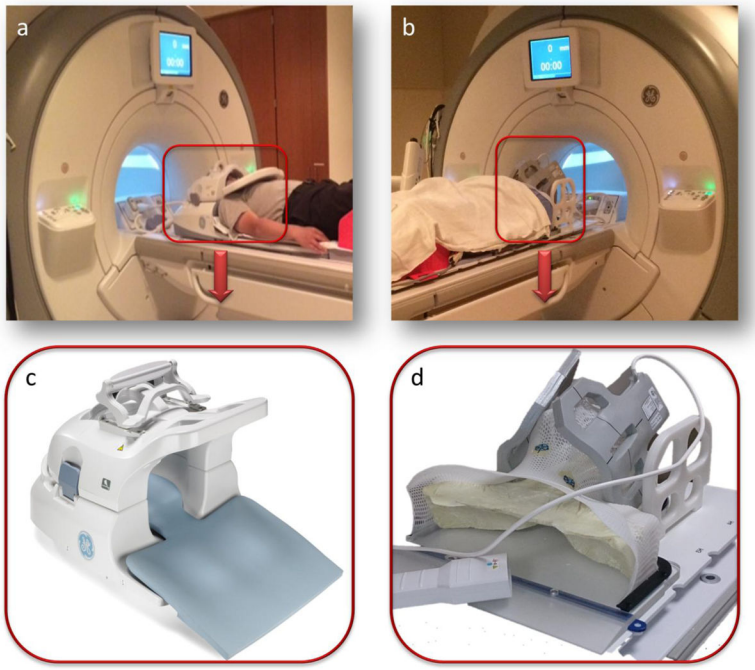

Fig. 1.

Photographs comparing the patient set-up applied for imaging with the neurovascular coil and standard diagnostic scan setup (a, c) for a patient in group 1 versus the flex coils and immobilization devices in “MR-simulation” method (b, d) for a patient in group 2.

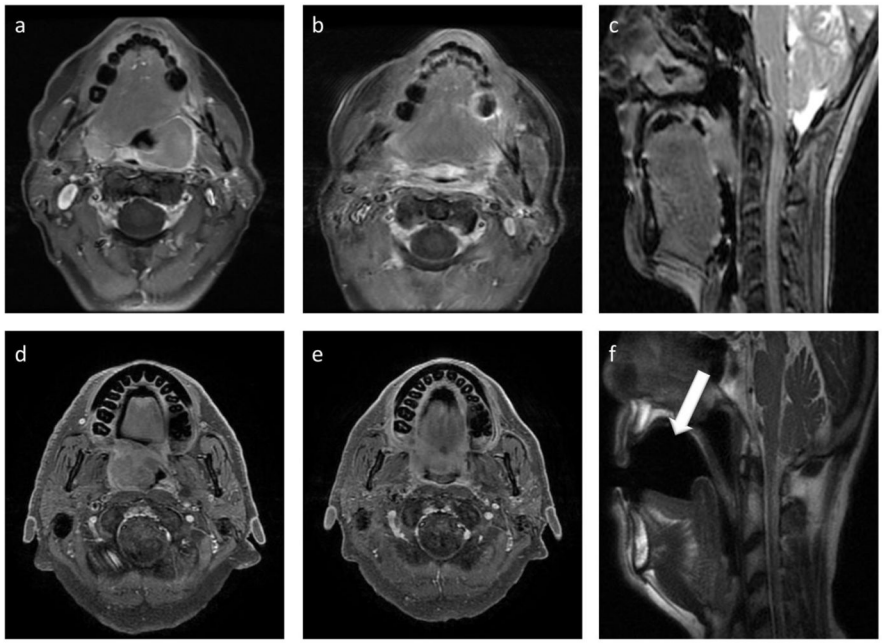

Fig. 2.

Post contrast T1-weighted images chosen from group 1 (upper panel) and group2 (lower panel) for image quality assessment. Axial images (a) and (d) represent pre-treatment while axial images (b) and (e) represent mid-treatment scans. Sagittal image (c) shows standard group 1 setup with no intra-oral dental stent while sagittal image (f) shows the “MR-simulation” setup with intra-oral dental stent (white arrow).

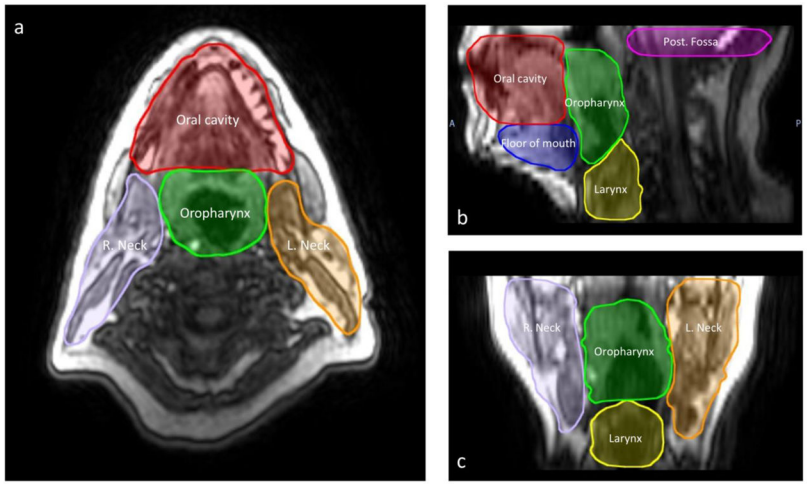

Fig. 3.

(a) Axial, (b) sagittal, and (c) coronal DCE-MRI of a head and neck patient, with the reference ROIs for tracking motion trajectory.

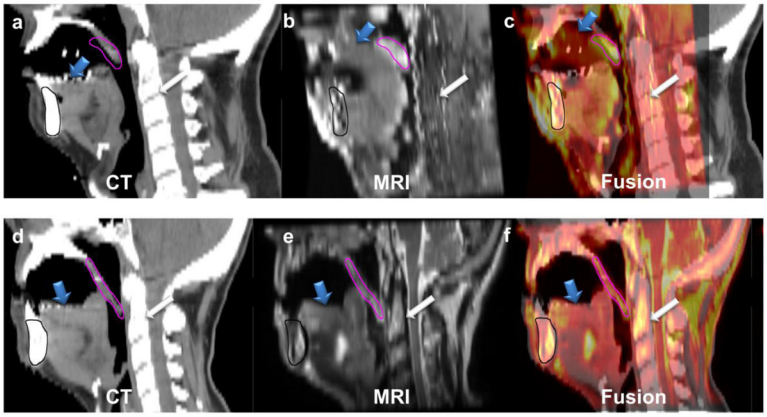

Fig. 4.

The upper panel shows the mid-sagittal sections of radiotherapy-simulation CT (a) registered to standard diagnostic MRI (b) with the fusion overlay (c) of a patient in group 1, while the lower panel shows the mid-sagittal sections of radiotherapy-simulation CT (d) registered to MRI acquired using the studied positioning and immobilization setup (e) with the fusion overlay (f) of a patient in group 2. The registration was done rigidly with priority to oral structures in both cases. It clearly illustrates the error in tongue (blue arrow), soft palate (pink contour segmented on MR and propagated to CT), and spine (white arrow) overlay in the case of group 1 compared to the case of group 2 despite perfect mandibular (black contour segmented on MR and propagated to CT) alignment.

Table 1

Guidelines for regions of interest (ROIs) segmentation.

ROI	Segmentation boundaries
Posterior cranial fossa	**Anteriorly:** clivus and petrous part of temporal bone
	Posterio-laterally: occipital bone
	Superiorly: tentorium cerebelli or first image acquisition when at lower level
	Inferiorly: foramen magnum
Oral cavity	**Anteriorly:** mucosa of upper and lower lips
	Posteriorly: level of palatoglossal folds (Ant. Pillars)
	Laterally: mucosa of the cheek
	Superiorly: hard palate
	Inferiorly: mucosa of the floor of mouth
Floor of mouth	**Antero-laterally:** mandible
	Posteriorly: posterior border of suprahyoid musculature
	Superiorly: mucosa of the floor of mouth
	Inferiorly: skin of the chin
Oropharynx	**Anteriorly:** level of palatoglossal folds (Ant. Pillars)
	Posterio-laterally: pharyngeal constrictors
	Superiorly: soft palate
	Inferiorly: upper surface of epiglottis
Larynx	**Anteriorly:** anterior border of thyroid cartilage
	Posterio-laterally: pharyngeal constrictors
	Superiorly: lower surface of epiglottis
	Inferiorly: lower border of cricoid cartilage
Right and left neck	**Anteriorly:** submandibular gland
	Posteriorly: posterior edge of sternomastoid muscle
	Medially: medial edge of carotids
	Laterally: skin of the neck
	Superiorly: lower edge of the lateral process of C1
	Inferiorly: lower border of cricoid cartilage

Table 2

Patients and disease characteristics.

Characteristics	Group 1 (n=17) N.	Group 2 (n=13) N.	*P*-value*
Age (y)			
Median (range)	54 (42–82)	58 (52–79)	0.24
Sex			
Male	15	13	0.20
Female	2	0	
T Stage			
T1	2	1	
T2	7	7	0.92
T3	5	3	
T4	3	2	
Tx	0	0	
N Stage			
N0	2	1	
N1	1	3	0.48
N2	14	10	
N3	0	0	
Nx	0	0	
Primary sites			
Base of Tongue	11	8	0.97
Tonsil	5	4	
Glossopharyngeal sulcus	1	1	

* *P* values were calculated with the use of Pearson's chi-square test for all comparisons, except age using 2-sample t-test.

Table 3

Image Quality Scores for Oropharyngeal Cancer MRI Protocols Assessed with and without using Immobilization Devices

Image quality score	Head motion Mean score (SD)		Tongue blur/ghosting Mean score (SD)		Reproducibility Mean score (SD)		Overall Mean score (SD)
	Ob1	Ob2	Ob1	Ob2	Ob1	Ob2	
Group 1 (50 scans)	1.85 (0.83)	1.98 (0.79)	1.59 (0.74)	1.75 (0.62)	1.65 (0.83)	1.47 (0.50)	1.72 (0.75)
Group 2 (29 scans)	2.54 (0.69)	2.79 (0.49)	2.43 (0.79)	2.55 (0.63)	2.63 (0.49)	2.57 (0.50)	2.58 (0.60)
***P* value**	<0.0002*	<0.0001*	<0.0001*	<0.0001*	<0.0001*	<0.0001*	<0.0001*

Abbreviations: Ob=Observer, SD=standard deviation

Table 4

Comparison of the greatest head and neck regional motion between groups

ROIs	Group 1† maximal displacement	Group 2‡ maximal displacement	*P*-value
	Mean (SD)	Mean (SD)	
Posterior cranial fossa	5.9 (3.5)	6.4 (4.1)	0.5
Oral cavity	11.9 (5.6)	5.1 (3.2)	<.0001*
Floor of mouth	12.7 (5.7)	7.5 (3.5)	<.0001*
Oropharynx	17.4 (7.9)	16.2 (7.5)	0.5
Larynx	18.6 (7.9)	16.4 (7.7)	0.2
Right neck	8.8 (5.3)	8.8 (4.2)	0.9
Left neck	12.0 (5.9)	10.5 (4.5)	0.2

Abbreviation: SD = standard deviation

† n = 50

‡ n = 29